

Methanol, ethanol and hydrogen sensing using metal oxide and metal (TiO₂–Pt) composite nanoclusters on GaN nanowires: a new route towards tailoring the selectivity of nanowire/nanocluster chemical sensors

Geetha S Aluri^{1,2}, Abhishek Motayed^{1,3}, Albert V Davydov¹, Vladimir P Oleshko¹, Kris A Bertness⁴, Norman A Sanford⁴ and Rao V Mulpuri²

¹ Material Measurement Laboratory, National Institute of Standards and Technology, Gaithersburg, MD 20899, USA

² Department of Electrical and Computer Engineering, George Mason University, Fairfax, VA 22030, USA

³ Institute for Research in Electronics and Applied Physics, University of Maryland, College Park, MD 20742, USA

⁴ Physical Measurement Laboratory, National Institute of Standards and Technology, Boulder, CO 80305, USA

E-mail: amotayed@nist.gov and amotayed@umd.edu

Received 21 November 2011, in final form 6 March 2012

Published 5 April 2012

Online at stacks.iop.org/Nano/23/175501

Abstract

We demonstrate a new method for tailoring the selectivity of chemical sensors using semiconductor nanowires (NWs) decorated with metal and metal oxide multicomponent nanoclusters (NCs). Here we present the change of selectivity of titanium dioxide (TiO₂) nanocluster-coated gallium nitride (GaN) nanowire sensor devices on the addition of platinum (Pt) nanoclusters. The hybrid sensor devices were developed by fabricating two-terminal devices using individual GaN NWs followed by the deposition of TiO₂ and/or Pt nanoclusters (NCs) using the sputtering technique. This paper presents the sensing characteristics of GaN/(TiO₂–Pt) nanowire–nanocluster (NWNC) hybrids and GaN/(Pt) NWNC hybrids, and compares their selectivity with that of the previously reported GaN/TiO₂ sensors. The GaN/TiO₂ NWNC hybrids showed remarkable selectivity to benzene and related aromatic compounds, with no measurable response for other analytes. Addition of Pt NCs to GaN/TiO₂ sensors dramatically altered their sensing behavior, making them sensitive only to methanol, ethanol and hydrogen, but not to any other chemicals we tested. The GaN/(TiO₂–Pt) hybrids were able to detect ethanol and methanol concentrations as low as 100 nmol mol⁻¹ (ppb) in air in approximately 100 s, and hydrogen concentrations from 1 μmol mol⁻¹ (ppm) to 1% in nitrogen in less than 60 s. However, GaN/Pt NWNC hybrids showed limited sensitivity only towards hydrogen and not towards any alcohols. All these hybrid sensors worked at room temperature and are photomodulated, i.e. they responded to analytes only in the presence of ultraviolet (UV) light. We propose a qualitative explanation based on the heat of adsorption, ionization energy and solvent polarity to explain the observed selectivity of the different hybrids. These results are significant from the standpoint of applications requiring

room-temperature hydrogen sensing and sensitive alcohol monitoring. These results demonstrate the tremendous potential for tailoring the selectivity of the hybrid nanosensors for a multitude of environmental and industrial sensing applications.

S Online supplementary data available from stacks.iop.org/Nano/23/175501/mmedia

(Some figures may appear in colour only in the online journal)

1. Introduction

The development of reliable, portable gas sensors that can detect harmful gases in real time with high sensitivity and selectivity is extremely important [1, 2]. In the last few decades significant advances have been made in the field of thin film sensors. Recently, there has been a tremendous interest in the development of nano-engineered materials, such as nanowires and nanoclusters, for gas sensing because of their high sensitivity [3–6]. Comprehensive reviews of metal, semiconductor and metal oxide nanowire-based gas sensors have been presented elsewhere [7, 8]. A detailed look at such reviews reveals that poor selectivity of these chemical sensors is still a major obstacle for commercializing nanoscale semiconducting gas sensors. For real-world applications, selectivity between different classes of compounds (such as between aromatic compounds and alcohols) is highly desirable. In fact, an ideal chemical sensor is one that can distinguish between the individual analytes belonging to a particular class of compounds, e.g. detection of the presence of benzene or toluene in the presence of other aromatic compounds. This is extremely challenging as most semiconductor-based sensors use metal oxides (such as SnO₂ or In₂O₃, ZnO) as the active elements, which are inherently limited due to the non-selective nature of the surface adsorption sites.

Recently, a new class of nanowire-based gas sensors has gained research interest. The nanowire–nanocluster (NWNC)-based gas sensors represent a way of functionalizing the surfaces of nanowires for selective adsorption and detection of analytes. They also offer the potential of tuning their sensitivity and selectivity by adjusting the composition, size and density of the nanoparticles, which makes them a good alternative to conventional metal-oxide-based thin film sensors [9, 10]. In recent years, researchers have demonstrated the potential of NWNC hybrids for sensing many different chemicals [11–15]. However, most of the hybrid devices developed so far require elevated working temperatures, have long response/recovery times, and operate in inert atmospheres, which limit their use in environmental, domestic and industrial applications.

We have recently demonstrated metal oxide nanoclusters (TiO₂) on GaN nanowires as a new architecture for highly selective gas sensing [16]. These hybrid sensors were capable of selectively sensing benzene and related aromatic compounds at the nmol mol⁻¹ (ppb) level in air at room temperature under UV excitation. In this paper, we present a new strategy for tailoring the selectivity of these nanowire–nanocluster (NWNC) hybrid sensors using

a multicomponent nanocluster design. Depositing catalytic metals such as Pt, Pd and other transition metals onto the surface of oxide photocatalysts is a well-known method for enhancing their catalytic activity. Metal clusters on metal oxide catalyst alter the behavior of the metal oxide catalyst by any one, or a combination of, the following mechanisms: (1) changing the surface adsorption behavior as metals often have very different heat of adsorption values compared to the metal oxides [17–19], (2) enabling catalytic decomposition of certain analytes on the metal surface, which otherwise would not be possible on the oxide surface [20], (3) transporting active species to the metal oxide support by the *spill-over* effect from the metal cluster [21], (4) generating a higher degree of interface states, thus increasing reactive surface area reaction area, (5) changing the local electronic properties of the metal clusters, such as workfunction, due to adsorption of gases [22] and (6) effectively separating photogenerated carriers in the underlying metal oxide [23]. The effect of transition metal loading such as Fe, Cu, Pt, Pd and Rh onto TiO₂ has also been extensively studied for photocatalytic decomposition of various chemicals in both gas–solid and liquid–solid regimes [24–26].

In this work we compare the sensing behavior of three NWNC-based hybrid sensors: (1) GaN NW coated with TiO₂ NCs (hereafter referred to as GaN/TiO₂ NWNC hybrids), (2) GaN NW coated with TiO₂ and Pt multicomponent NCs (i.e. GaN/(TiO₂–Pt) NWNC hybrids) and (3) GaN NW coated with Pt NCs (i.e. GaN/Pt NWNC hybrids). We found that sensors with TiO₂–Pt multicomponent NCs on GaN NW were only sensitive to methanol, ethanol and hydrogen. Higher carbon-containing alcohols (such as n-propanol, iso-propanol, n-butanol) did not produce any sensor response. These sensors have the highest sensitivity towards hydrogen. Prior to the Pt deposition, the GaN/TiO₂ NWNC hybrids did not exhibit any response to alcohols: however, they detected benzene and related aromatic compounds such as toluene, ethylbenzene, xylene and chlorobenzene mixed with air. The GaN/Pt hybrids only showed sensitivity to hydrogen and not to methanol or ethanol. The sensitivity of GaN/Pt hybrids towards hydrogen was lower compared to the GaN/(TiO₂–Pt) hybrids.

Tables 1 and 2 compare the performance of our sensor devices with the most recent literature in terms of operational temperature, carrier gas, lower detection limit and response/recovery times. Though the literature study is not exhaustive, the comparison is intended to show that our sensor devices have good response to very low concentrations of analytes (100 ppb for ethanol and 1 ppm for hydrogen) at room temperature, with air as the carrier gas. This testing condition closely resembles the real-life conditions, which

Table 1. Performance of GaN/(TiO₂-Pt) NWNC hybrid sensors to ethanol in comparison with recent literature.

	Response/recovery times	Lower detection limit	Carrier gas	Temperature	References
Our sensor	80/75 s	100 ppb with 1% sensitivity ^a	Air	Room temperature (RT)	—
CNT ^b /SnO ₂ core-shell nanostructures	1/10 s	10 ppm	Air	300 °C	[27]
MWCNTs ^c /NaClO ₄ /polypyrrole	20/20 s	18 000 ppm	Air	RT	[28]
Metal-CNT hybrids	~2 min/not-mentioned (NM)	500 ppb with sensitivity <1%	N ₂ in a vacuum test chamber	RT	[29]
V ₂ O ₅ nanobelts	50/50 s	5 ppm	Air	150–400 °C	[30]
ZnO nanorods	3.95/5.3 min	10 ppm	Synthetic air	125–300 °C	[31]
ZnO nanowires	10/55 s	1 ppm	Air	220 °C	[32]
ITO ^d nanowires	2/2 s	10 ppm	Air	400 °C	[33]
SnO ₂ nanowires	2/2 s	10 ppm	Air	300 °C	[34]

^a We only compared the sensitivity values for sensors with the lowest detection limit similar to our result.

^b Carbon nanotubes.

^c Multi-wall carbon nanotubes.

^d Indium tin oxide.

Table 2. Performance of GaN/(TiO₂-Pt) NWNC hybrid sensors to hydrogen in comparison with recent literature.

	Response/recovery times	Lower detection limit	Temperature	Reference
Our sensor	60/45 s	1 ppm with sensitivity of 4%	RT	—
CNT films	5 min/30 s	10 ppm	RT	[35]
SWCNT/SnO ₂	2/2 s	300 ppm	250 °C	[36]
Pd/CNTs	5/5 min	30 ppm with sensitivity of 3%	RT	[37]
Pd/Si NWs	1 h/50 min	3 ppm	RT	[38]
Pt-doped SnO ₂ NWs	2/10 min	100 ppm	100 °C	[39]

underlines the significance of this study. The response and recovery times are also lower for our sensors compared to most other sensors in tables 1 and 2.

The present results point towards the unique possibility of tailoring the selectivity of NWNC chemical sensors. With infinite combinations of metal and metal oxide composite clusters available, there is a huge potential for sensor designs targeted for a multitude of applications.

2. Experimental details

The GaN NWs used in this study were *c*-axis, *n*-type (Si-doped), grown by catalyst-free molecular beam epitaxy as described elsewhere [40]. Post-growth device fabrication was done by dielectrophoretically aligning the nanowires on 9 mm × 9 mm sapphire substrates. The details of the device fabrication including the process flow diagram can be found in our previous paper [16]. After fabrication of two-terminal GaN NW devices, the TiO₂ NCs were deposited on the GaN NW surface using RF magnetron sputtering. The deposition was done at 325 °C with 50 standard cubic centimeters per minute (sccm) of Ar flow and 300 W RF power. The nominal deposition rate was about 0.24 Å s⁻¹. Thermal annealing of the complete sensor devices (GaN NW

with TiO₂ nanoclusters) was done at 700 °C for 30 s in a rapid thermal processing system. For TiO₂-Pt composite NCs, the Pt was sputtered using DC sputtering after annealing of the TiO₂ clusters on GaN NW. The Pt sputtering was done with an Ar flow of 35 sccm, at a pressure of 1.3 Pa and power of 40 W for 10 s. For the Pt/GaN devices Pt was sputtered on bare GaN NWs after annealing the ohmic contacts at 700 °C for 30 s. Additional lithography was performed to form thick metal bond pads with Ti (40 nm) and Au (200 nm). The device substrates, i.e. the *sensor chips*, were wire-bonded on a 24-pin ceramic package for the gas sensing measurements.

The microstructure and morphology of the sputtered TiO₂ films used for the fabrication of the sensors were characterized by high-resolution transmission and scanning transmission electron microscopy (HRTEM/STEM), selected-area electron diffraction (SAED) and field-emission scanning electron microscopy (FESEM). For the TEM characterization, the GaN NWs were dispersed on 10 nm thick carbon films supported by Mo mesh grids, followed by the deposition of TiO₂ NCs and annealing, and subsequent Pt deposition. The samples were analyzed in a FEI Titan 80-300 TEM/STEM microscope operating at 300 kV accelerating voltage and equipped with S-TWIN objective lenses, which provided 0.13 nm (STEM)

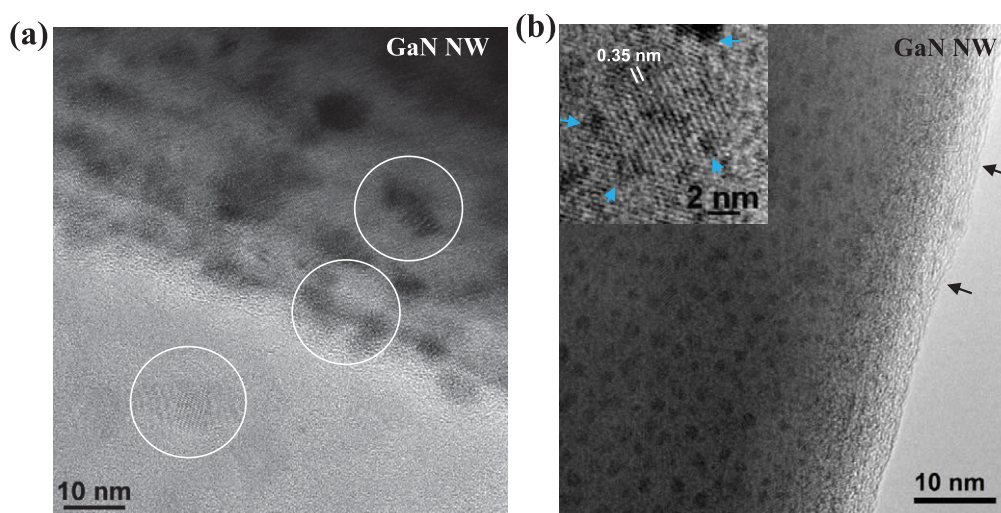


Figure 1. HRTEM image of a GaN NW with TiO₂ sputtered on them: (a) before Pt and (b) after Pt deposition. White circles in (a) indicate partially aggregated polycrystalline TiO₂ particles on the NW surface and on the supporting carbon film. Blue arrows (image (b), top left enlarged inset) mark Pt clusters decorating a 6 nm diameter particle of titania. The TiO₂ particle exhibits 0.35 nm fringes corresponding to (101) lattice spacing of anatase polymorph. 2–5 nm thick amorphized surface film indicated by black arrows is also shown.

and 0.19 nm (TEM) resolution by points⁵. The instrument also had a Gatan CCD image acquisition camera, bright-field (BF), ADF and high-angle annular dark-field (HAADF) STEM detectors to perform spot, line profile and areal compositional analyses using an EDAX 300 kV high-performance Si/Li x-ray energy dispersive spectrometer (XEDS).

The as-fabricated sensors were placed in a custom-designed gas chamber for gas exposure measurements. Detailed description of the experimental set-up and experimental conditions can be found in an earlier paper [16]. The device characterization and the time-dependent sensing measurements were done using an Agilent B1500A semiconductor parameter analyzer. The gas sensing experiments have been performed by measuring the electrical conductance of the devices upon exposure to controlled flow of an air/chemical mixture in the presence of UV excitation (25 W deuterium bulb operating in the 215–400 nm range). For all the sensing experiments with chemicals, breathing air ($<9 \mu\text{mol mol}^{-1}$ of water) was used as the carrier gas. For the hydrogen sensing we used high-purity nitrogen as the carrier gas. After the sensor devices were exposed to the organic compounds and hydrogen, they were allowed to regain their baseline current with the air–chemical mixture turned off, without purging or evacuating the test chamber.

3. Results

3.1. Morphological and structural characterization of NWNC hybrids

It is challenging to measure the sizes and shapes of small TiO₂ and Pt particles on the surface GaN NWs from

grayscale TEM images due to: (a) 270–300 nm thickness of the NWs used in the devices and variations of thickness and curvature across the structure; (b) diffraction contrast induced particularly by bending of the wires: even similar particles could appear as having different intensities, while local thickness variations of the carbon support film could result in variable contrast affecting the mean intensity values of the particles; and (c) overwhelming domination of electron diffraction in SAED from the GaN NW over the diffraction from TiO₂ and Pt nanoparticles. To overcome these problems, TEM imaging was conducted under minimal beam intensity conditions close to the Scherzer defocus at a highest available accelerating voltage of 300 kV using both stationary beam (bright-field TEM/SAED, phase-contrast high-resolution TEM) and scanning beam (STEM/XEDS) modes. Areas for analyses were selected near the wire's edges and on the amorphous carbon support film in the vicinity of the NWs.

Figure 1 shows HRTEM micrographs of a GaN NW on thin amorphous carbon support films with TiO₂ coating, before and after the Pt deposition. The deposited TiO₂ layer formed an island-like film, where 10–50 nm partially aggregated particles (see figure 1(a)) were often interconnected into extended two-dimensional networks. This was consistent with SAED and compositional analyses of deposited TiO₂ films, indicating a mixture of polycrystalline anatase and rutile and of the same mixture plus fcc Pt nanoparticles (figure 1(b)), respectively (see supplementary data for details available at stacks.iop.org/Nano/23/175501/mmedia). Pt crystalline particles with 1–5 nm size were randomly distributed on the surfaces of TiO₂ islands and sometimes were partially coalesced forming elongated aggregates. In the latter case, a significant thickness of the GaN NWs made it difficult to visualize TiO₂ deposits due to the limited contrast difference between TiO₂ and GaN and the presence of multiple heavy Pt particles. In spite of these severe limitations, detailed HRTEM and HR-STEM observations

⁵ Certain commercial equipment, instruments or materials are identified in this paper to foster understanding. Such identification does not imply recommendation or endorsement by the National Institute of Standards and Technology nor does it imply that the materials or equipment identified are necessarily the best available for the purpose.

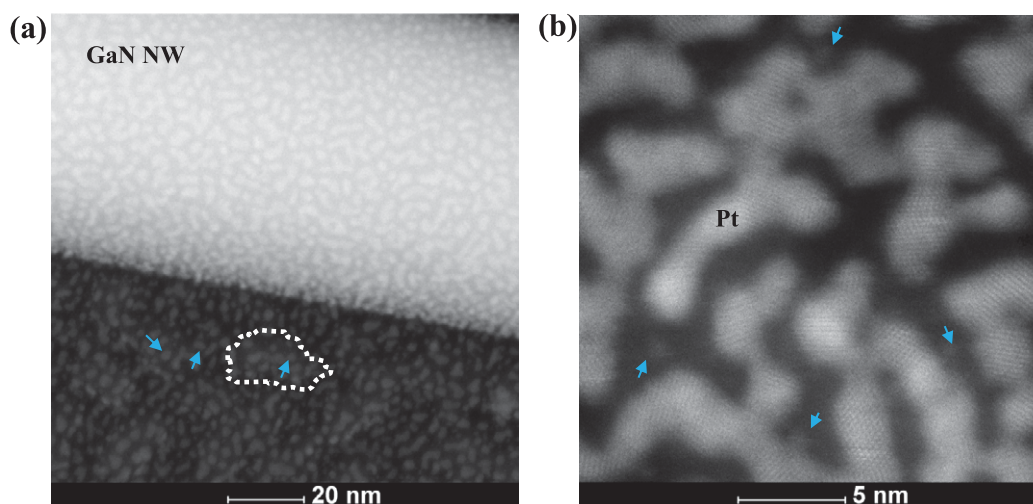


Figure 2. HAADF-STEM of a GaN NW coated with TiO_2 and Pt. (a) 1–5 nm bright Pt nanoparticles (shown by blue arrows) decorating surfaces of a polycrystalline TiO_2 island-like film and of a GaN nanowire. Medium gray aggregated TiO_2 particles (outlined by dashed white line in (a)) are barely visible on a thin carbon support in image (a) near the edge of the nanowire. (b) High magnification image of the supporting film near the edge of the nanowire exhibits 0.23–0.25 nm (111) and 0.20–0.22 nm (200) fcc lattice fringes belonging to Pt nanocrystallites; blue arrows indicate amorphous-like Pt clusters of 1 nm or less in diameter.

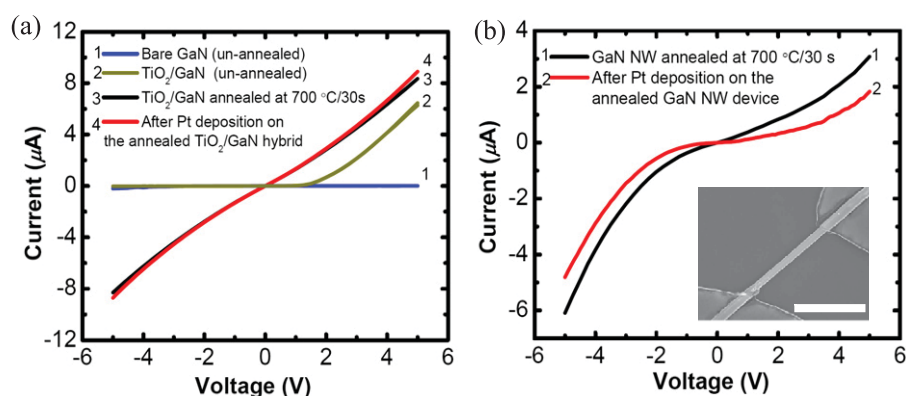


Figure 3. I – V characteristics of the hybrid sensor device at different stages of processing: (a) GaN/ $(\text{TiO}_2$ –Pt) hybrids and (b) GaN/Pt hybrids. Inset in (b) shows the plan-view SEM image of a typical GaN NWNC hybrid sensor. The scale bar in the inset is 4 μm .

revealed 0.35 nm (101) hcp lattice fringes belonging to anatase (see figure 1(b), inset) and 0.23–0.25 nm (111) and 0.20–0.22 nm (200) fcc lattice fringes belonging to Pt nanocrystallites, respectively, as well as amorphous-like Pt clusters with diameter around 1 nm or less (see figures 2(a) and (b)).

In figure 2 HAADF-STEM image shows 1–5 nm diameter bright Pt nanoparticles and barely visible TiO_2 islands (medium gray) randomly distributed near the edge of the nanowire. The presence of both TiO_2 and Pt nanocrystallites was confirmed by the analysis of selected areas using XEDS nanoprobe capabilities (see supplementary data available at stacks.iop.org/Nano/23/175501/mmedia).

3.2. Current–voltage (I – V) characteristics of NWNC hybrids in dark

Figure 3 shows the I – V characteristics of the GaN/ $(\text{TiO}_2$ –Pt) and GaN/Pt hybrid sensor devices at different stages of processing. The plan-view SEM image of a typical sensor

device is shown in the inset of figure 3(b) for representation purpose. The I – V curves of the as-fabricated GaN NW two-terminal devices were nonlinear and asymmetric (not clear in figure 3(a) due to scale resolution). A small increase in the positive current after the deposition of TiO_2 nanoclusters (curve 2) can be attributed to decreased surface depletion of the GaN NWs due to passivation of surface states and/or the high-temperature deposition (325 °C) of the nanoclusters initiating ohmic contact formation. The devices annealed at 700 °C for 30 s after the deposition of TiO_2 NCs showed significant change in their I – V characteristics with a majority of the devices exhibiting linear I – V curves. Interestingly, Pt NC deposition on TiO_2 -coated GaN NWs further increased the conductivity of the nanowire. This is probably due to the fact that the Pt clusters depleted the TiO_2 clusters by removing free electrons; increased depletion in the TiO_2 clusters due to Pt would decrease TiO_2 -induced depletion in the GaN NW, leading to an increase in the NW current. With the Pt/GaN hybrids, the current decreases followed by the deposition of Pt (figure 3(b)), as expected due to the

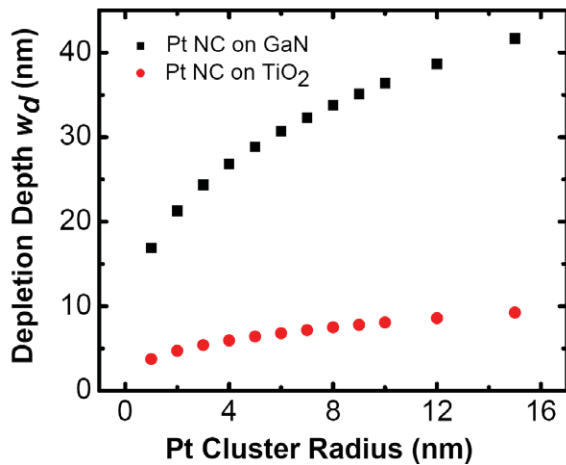


Figure 4. Depletion depth induced by Pt NCs on GaN and TiO₂ as calculated by equation (1).

depletion region formed in the NW under the metal clusters. It is worthwhile to discuss the nature of the depletion region formed by such nanosized metal clusters on a semiconductor. It has been shown that the classical Schottky model depletion theory cannot predict accurately the zero-bias depletion width produced by metallic nanoclusters on a semiconductor [41]. According to Zhdanov's model the depletion depth associated with such metal nanoclusters on a semiconductor can be estimated by the relationship [42]:

$$w_d = \left(\frac{3r_c V_{bi}}{2\pi q^2 N_d} \right)^{1/3} \quad (1)$$

where w_d is the depletion width, r_c is the radius of the nanocluster, V_{bi} is the built-in voltage for the GaN–Pt junction, q is the elementary charge and N_d is the dopant concentration in the nanowire. Figure 4 shows the calculated zero-bias depletion depth produced in GaN and TiO₂, respectively, as a function of the Pt cluster radius according to equation (1). For calculating the depletion depth we assumed the effective conduction band density of states in TiO₂ as $3.0 \times 10^{21} \text{ cm}^{-3}$ and point-defect-related donor concentration

as $1.0 \times 10^{18} \text{ cm}^{-3}$ [43, 44]. The electron concentration in the GaN NWs was measured to be $1 \times 10^{17} \text{ cm}^{-3}$ in a separate experiment.

Figure 4 indicates that even a single Pt NC of 2 nm radius can significantly deplete a 10 nm (average size) TiO₂ cluster. The effect of TiO₂ depletion on GaN NW is hard to compute as it could be influenced by numerous factors including interface states and the particle geometry. Given the very high density of TiO₂ clusters on the NW surface (see figure 2(b)), it is clear that the Pt particles mostly reside on the surfaces of TiO₂ NCs. However, from figure 4 we can see that, when Pt NCs are directly on GaN, they should deplete the carriers in an even larger region in the GaN NW. This qualitatively explains the relatively larger change in current observed when Pt NCs were deposited on bare GaN NWs as compared to the change in current when Pt NC were deposited on the TiO₂-coated NWs.

3.3. Comparative sensing behavior of GaN/(TiO₂–Pt), GaN/Pt and GaN/TiO₂ NWNC hybrid sensors

The photocurrent through the bare GaN NW devices did not change when exposed to different chemicals mixed in air, even for concentrations as high as 3%. In contrast, the TiO₂-coated hybrid devices responded even to the pulses of 20 sccm airflow in the presence of UV excitation. The response of the TiO₂ NC-coated GaN nanowire hybrid sensors to different concentrations of benzene, toluene, ethylbenzene, chlorobenzene and xylene in air is illustrated in our earlier paper and will not be discussed here [16]. The GaN/TiO₂ hybrids showed no response when exposed to other chemicals such as alcohols, ketones, amides, alkanes, nitro/halo-alkanes and esters.

Remarkably, after the deposition of Pt nanoclusters on the GaN/TiO₂ hybrids, the sensors were no longer sensitive to benzene and other aromatic compounds, but responded only to hydrogen, methanol and ethanol. In addition, the GaN/(TiO₂–Pt) hybrids showed no response when exposed to higher carbon-containing ($C > 2$) alcohols such as n-propanol, iso-propanol and n-butanol. Figure 5 shows the change of photocurrent of a GaN/(TiO₂–Pt) sensor

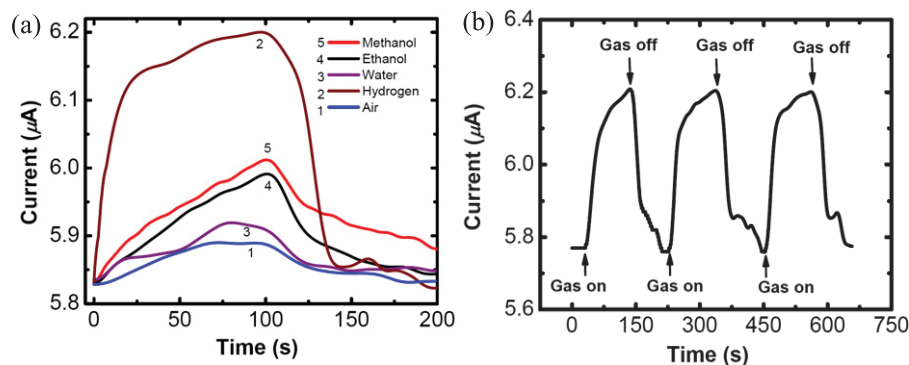


Figure 5. (a) UV photo-response of the GaN/(TiO₂–Pt) hybrid device to 1000 $\mu\text{mol mol}^{-1}$ (ppm) of methanol, ethanol and water in air, and hydrogen in nitrogen. The air–gas mixture was turned on at 0 s and turned off at 100 s. (b) Cyclic response of the GaN/(TiO₂–Pt) hybrid device when exposed to 2500 $\mu\text{mol mol}^{-1}$ (ppm) of hydrogen in nitrogen. The bias voltage for all the devices was 5 V.

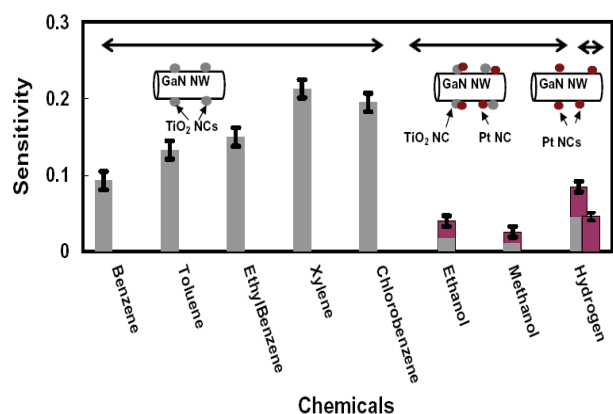


Figure 6. Comparative sensing behavior of the three hybrids for $1000 \mu\text{mol mol}^{-1}$ (ppm) of analyte in air: gray bar graphs represent GaN/TiO₂ hybrids, gray and maroon represent GaN/(TiO₂-Pt) hybrids, and maroon plot represents GaN/Pt hybrids. Other chemicals which did not produce any response in any one of the hybrids are not included in the plot. The zero line is the baseline response to 20 sccm of air and N₂. For this plot the magnitude of the sensitivity is used. The error bars represent the standard deviation of the mean sensitivity values for every chemical computed for five devices with diameters in the range of 200–300 nm.

in the presence of 20 sccm air flow of air mixed with $1000 \mu\text{mol mol}^{-1}$ (ppm) of methanol, ethanol and water, respectively, and 20 sccm of nitrogen flow mixed with $1000 \mu\text{mol mol}^{-1}$ (ppm) hydrogen. The change in the photocurrent of the sensor when 20 sccm of breathing air is flowing through the test chamber serves as a reference for calculating the sensitivity of the sensors. We have defined the sensitivity as $(R_{\text{gas}} - R_{\text{air}})/R_{\text{air}}$, where R_{gas} and R_{air} are the resistances of the sensor in the presence of the analyte–air mixture and in the presence of air only, respectively (R_{air} is replaced with R_{nitrogen} for hydrogen sensing experiments).

It is worth mentioning that the GaN/TiO₂ hybrids without Pt showed no response to hydrogen and the alcohols. Interestingly, when Pt NC-coated GaN NW hybrids (GaN/Pt) with the same nominal thickness were tested, they showed very limited sensitivity only to hydrogen and not to any alcohols. The comparative summary of the sensing behavior of the three different hybrids are presented in figure 6.

The response of the GaN/(TiO₂-Pt) NWNC sensors to different concentrations of methanol in air is shown in figure 7(a). Figure 7(b) shows the response to different concentrations of hydrogen in nitrogen for the same sensor device. The sensor response is much higher for hydrogen compared to methanol and ethanol. The response time is also much shorter for hydrogen as compared to methanol and the sensor photocurrent saturates after an initial 20 s exposure.

The response time was arbitrarily defined as the time taken by the sensor current to reach 90% of the response ($I_f - I_0$) when exposed to the analyte. The I_f is the steady sensor current level in the presence of the analyte and I_0 is the current level without the analyte, which in our case is in the presence of 20 sccm of air flow. The recovery time is the time required for the sensor current to recover to 30% of the response ($I_f - I_0$) after the gas flow is turned off [45]. The response time for hydrogen is ≈ 60 s, whereas the response time for ethanol and methanol is ≈ 80 s. The sensor recovery time for hydrogen is ≈ 45 s and the recovery times for ethanol and methanol are ≈ 60 s and ≈ 80 s, respectively. For comparison, Wang *et al* demonstrated a ZnO NW-based hydrogen sensor with a response time of 10 min for 4.2% sensitivity [46]. The ZnO NW-based hydrogen sensor reported by Lupan *et al* showed a sensitivity of 34% for a response time of 64 s [47].

The sensitivity plot of a GaN/(TiO₂-Pt) hybrid device for the various analytes tested is shown in figure 8(a). It is to be noted that the lowest concentration detected for methanol and hydrogen (1 ppm or $\mu\text{mol mol}^{-1}$) is not the sensor's detection limit, but a system limitation. It can be seen that the sensor is more sensitive to methanol than ethanol for concentrations $\geq 1000 \mu\text{mol mol}^{-1}$ (ppm), and the relative sensitivity switches for concentrations of $500 \mu\text{mol mol}^{-1}$ (ppm) and below. Similar behavior is observed with 20 unique devices, possibly due to differences in surface coverage of the different alcohols over the concentration range. Figure 8(b) is a comparative plot showing the sensitivity of GaN/(TiO₂-Pt) and GaN/Pt hybrid sensors to hydrogen in nitrogen. The GaN/Pt hybrid devices showed relatively low sensitivity with detection limit of $50 \mu\text{mol mol}^{-1}$ (ppm), below which the devices stopped responding. The gas exposure time was also increased to 200 s for the GaN/Pt devices to obtain increased

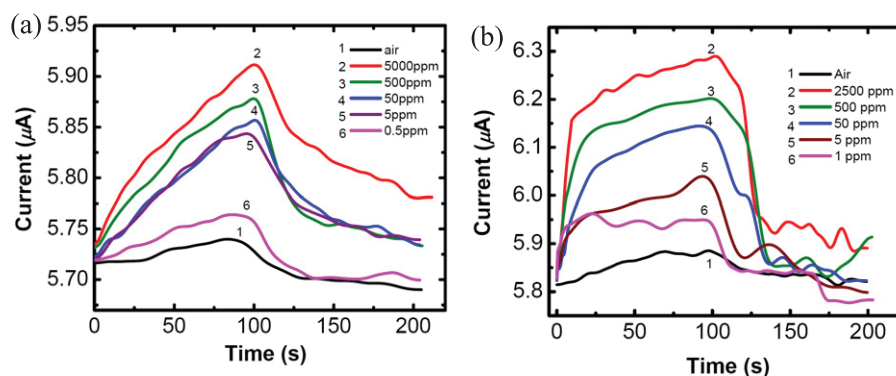


Figure 7. (a) Photo-response of GaN/(TiO₂-Pt) hybrid device to different concentrations of methanol in air. (b) Photo-response of the same device to different concentrations of hydrogen in nitrogen. The air–gas mixture was turned on at 0 s and turned off at 100 s.

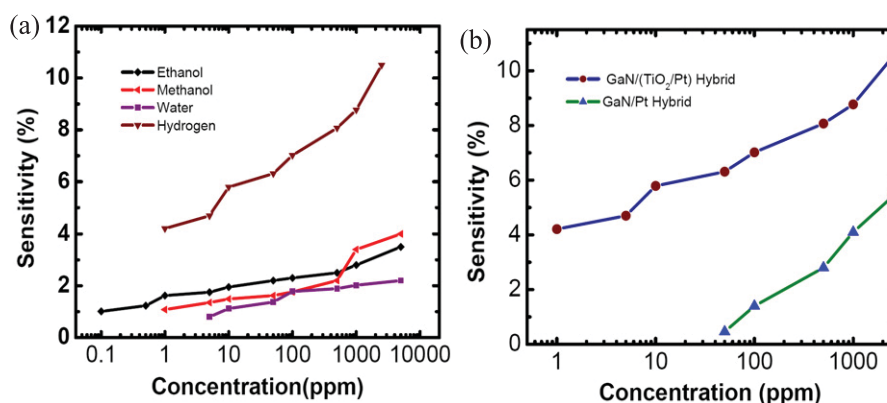


Figure 8. (a) Sensitivity plot of the GaN/(TiO₂-Pt) hybrid device to ethanol, methanol and water in air and to hydrogen in nitrogen ambient. (b) Comparison of the sensitivity of GaN/(TiO₂-Pt) and GaN/Pt devices to different concentrations of hydrogen in nitrogen.

response compared to 100 s for the GaN/(TiO₂-Pt) GaN devices. The sensitivity of the GaN/(TiO₂-Pt) sensors is greater for alcohols and hydrogen when compared with the same concentrations of water in air, which should enable their use in high-humidity conditions.

4. Discussion

In section 3.3 we presented the detailed sensing performance of three different NWNC sensors. Understanding the exact selective sensing mechanism is complicated. However, a qualitative understanding can be developed considering how different molecules adsorb on the nanocluster surfaces, and determining the roles of intermediate reactions in the sensitivity of the NWNC sensors.

4.1. The photocurrent in GaN/(TiO₂-Pt) hybrid sensors in the presence of air, nitrogen and water

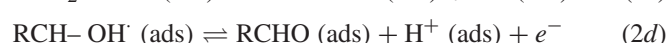
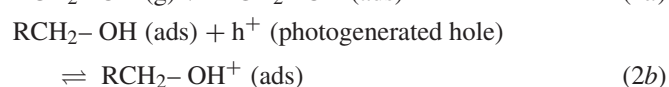
It is well established that the oxygen vacancy defects (Ti³⁺ sites) on the surface of TiO₂ are the 'active sites' for the adsorption of species like oxygen, water and organic molecules [48, 49]. It has been observed that oxygen adsorption on photocatalyst powders such as TiO₂ and ZnO quenches the PL intensity, while adsorption of water produces an enhancement of the PL. Mayer *et al* [50] and Anpo *et al* [51] proposed that electron-trapping adsorbates, such as oxygen, increase the band bending of TiO₂, which facilitates the separation of photogenerated electron-hole pairs in the oxide. Subsequently the PL intensity is decreased as the photogenerated charge carriers cannot recombine efficiently. Conversely, in the case of water, the band bending is reduced, resulting in an increase in the PL intensity. In explaining the observed behavior of the hybrid sensors, we also have to consider the depletion effect induced by the TiO₂ clusters on the GaN NW, which is complicated. Considering an inverse relationship, i.e. increase in depletion of the TiO₂ cluster leads to a decrease in the depletion width in the GaN NW and vice versa, we can explain some of the observed sensing behavior. As depicted in figure 9, when oxygen is adsorbed on the TiO₂ NC surface, the depletion width in the NC

increases, leading to a decrease in the depletion width in the NW. Adsorption of water, nitrogen and alcohol produce the reverse effect: they decrease the depletion width of the TiO₂ NC, leading to an increase in the band bending on the GaN NW. Increased band bending in the GaN NW would result in an effective separation of charge carriers, leading to an increase in photocurrent through the NW. This qualitatively explains the increase in the photocurrent when the hybrid sensor is exposed to water mixed with air or with pure nitrogen (figure 10). However, it fails to explain the increase in the photocurrent when exposed to 20 sccm of air flow. Under air flow, more oxygen should adsorb on the NCs, causing an increase in the depletion width of the cluster. This should have resulted in a decrease in the photocurrent based on our assumption; however, we see an increase in the photocurrent (figure 10) when 20 sccm of air is passed through the chamber. The reason for this is not clear at this time.

In the absence of UV light, the absorption or desorption of chemicals from the cluster surfaces cannot modulate the dark current through the nanowire. In dark, the surface depletion layer of the GaN NW is thicker compared to under UV excitation [52], and also the minority carrier (hole) concentration is significantly lower. Thus the NCs are ineffective in modulating the dark current through the NW.

4.2. Mechanism of sensing of alcohols and hydrogen by GaN/(TiO₂-Pt) NWNC sensors

Adsorption of alcohols (RCH₂-OH) on a TiO₂ surface can lead to their oxidation [53]. Although there are various mechanisms of oxidation of adsorbed alcohols on a TiO₂ surface, we will focus on the oxidation of alcohols by photogenerated holes. The process can be described by the following reactions [53]:



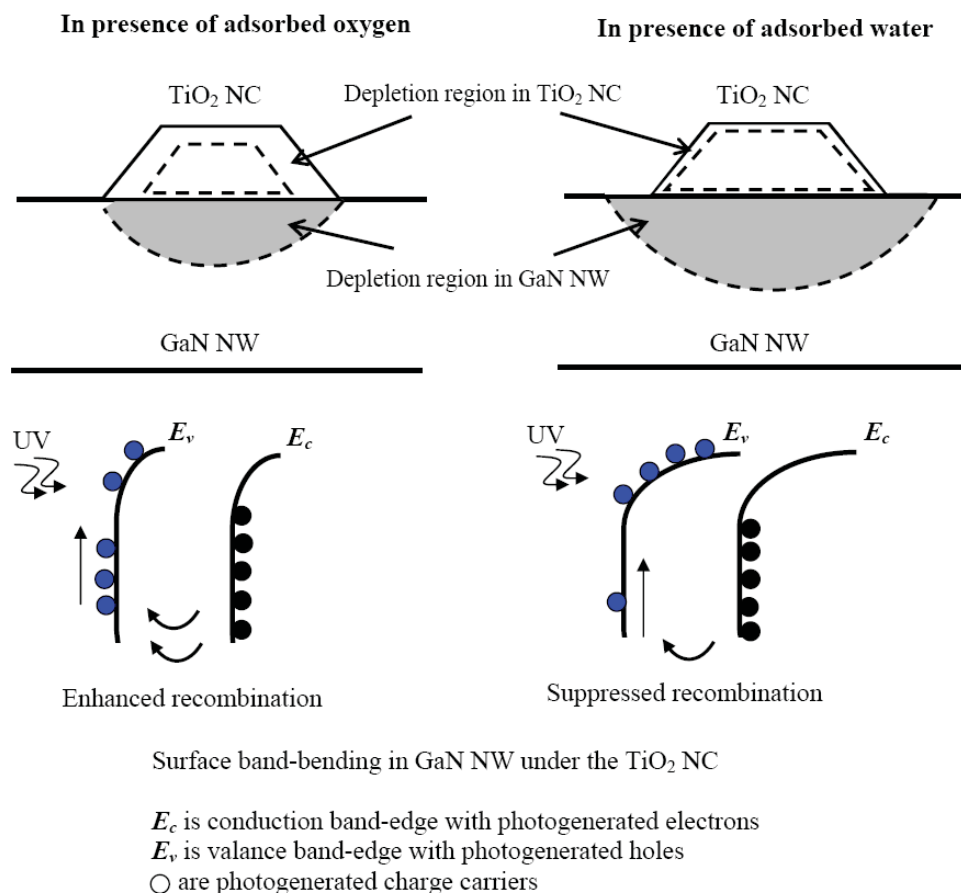
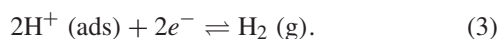


Figure 9. Schematic representation of the depletion in the TiO₂ NC in the presence of oxygen and water, and its effect on the photogenerated charge carrier separation in GaN NW. Circles in valence band indicate holes and circles in conduction band indicate electrons.

where (ads) and (g) represent adsorbed and gas phase species, respectively. For equation (2d) to proceed in the forward directions, the H⁺ species should be removed effectively. It is possible that from TiO₂ NCs the H⁺ species can *spill-over* onto Pt clusters nearby, where they can be reduced to form H₂:



As H⁺ reduction and hydrogen–hydrogen recombination is weak on the bare TiO₂ surface [54], the rate of alcohol oxidation to aldehyde might be affected by the H⁺ reduction and hydrogen–hydrogen recombination on the Pt NCs. Adsorption of alcohols and their subsequent oxidation due to trapping of photogenerated holes leads to a decrease in the band bending of TiO₂ NCs. This, according to figure 9, will lead to an increase in the NW photocurrent, which is observed for the GaN/(TiO₂–Pt) sensors when exposed to methanol and ethanol (figure 10). It is likely that the production of H₂ on Pt is the key for sensing alcohols by GaN/(TiO₂–Pt) sensors. Additionally, H₂ on a Pt surface can dissociate and diffuse to the Pt/TiO₂ interface. Atomic hydrogen is shown to produce an interface dipole layer, which reduces the effective workfunction of Pt [55]. Effective reduction of Pt workfunction might also reduce the depletion width in TiO₂, which, according to the model in figure 9, would also lead to an increase in the photocurrent, when these sensors

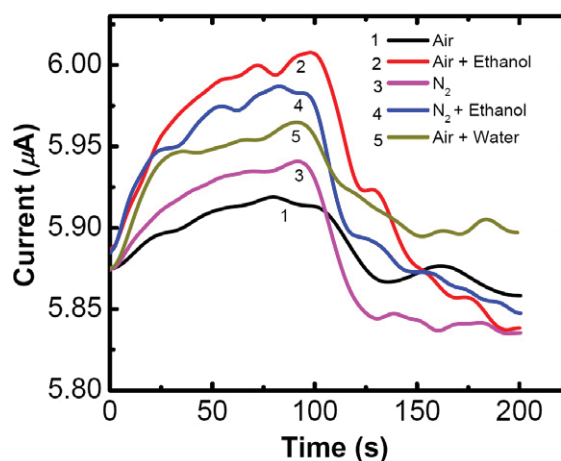


Figure 10. Photo-response of the GaN/(TiO₂–Pt) device to 1000 µmol mol^{−1} of ethanol in air and nitrogen, and to 1000 µmol mol^{−1} of water in air. The devices did not respond to water in nitrogen. The air–gas mixture was turned on at 0 s and turned off at 100 s.

are exposed to alcohols. In the presence of hydrogen in nitrogen, the workfunction change of Pt NCs due to hydrogen adsorption is the most likely cause for the sensing behavior of these hybrids.

Table 3. Heat of adsorption for methanol, benzene and hydrogen on Pt and TiO₂ (anatase) (Note: the heat of adsorption values for TiO₂ rutile surfaces are comparable.)

Surface	Hydrogen (kJ mol ⁻¹)	Methanol (kJ mol ⁻¹)	Benzene (kJ mol ⁻¹)
TiO ₂	Negligible [56]	92 [57]	64 [58]
Pt	100 [59]	48 [60]	117 [61]

Table 4. Ionization energy of the analytes [62].

Organic compound	Ionization energy (eV)
Methanol	10.85
Hydrogen	13.5
Benzene	9.25

4.3. Selectivity of GaN/(TiO₂-Pt), GaN/Pt and GaN/TiO₂ NWNC hybrid sensors

The most significant finding of this study is the change in the selectivity of GaN/TiO₂ hybrid sensors due to addition of Pt NCs. The observed selectivity behavior of the three hybrids can be qualitatively explained if we consider the heat of adsorption of the analytes on TiO₂ and Pt surfaces as seen in table 3 and their ionization energies presented in table 4.

The selectivity of the different hybrids required can be better explained if we answer the following four questions.

(1) Why can benzene be detected only by GaN/TiO₂ hybrids, but not by the GaN/(TiO₂-Pt) and GaN/Pt devices?

Looking at table 3, benzene has a higher heat of adsorption on Pt than on TiO₂. Therefore, benzene will preferentially adsorb on Pt in the TiO₂-Pt cluster. Now, in the absence of Pt, when the benzene is adsorbed on TiO₂ it can interact with the photogenerated charge carriers, resulting in the sensing behavior of GaN/TiO₂ devices. However, if benzene is adsorbed on Pt (such as in the case of TiO₂-Pt and Pt nanoclusters on GaN) then benzene molecules cannot interact with photogenerated charge carriers in TiO₂ and therefore are ineffective in producing any current modulation in the nanowire.

(2) Why is methanol detected by GaN/(TiO₂-Pt) sensors only, and not by GaN/TiO₂ and GaN/Pt sensors?

From table 3, methanol (unlike benzene) effectively adsorbs on TiO₂, whether Pt is present or absent (as the heat of adsorption of methanol is higher on TiO₂ than Pt). It is possible that methanol on TiO₂ in the absence of Pt does not participate in photogenerated carrier trapping as efficiently as benzene and other aromatic compounds on the TiO₂ nanoclusters. Table 4 shows the ionization energy of methanol, hydrogen and benzene. The effectiveness of the process of hole transfer to the adsorbed organic molecules should be related to the compound's ability to donate an electron (i.e. the lower the ionization energy of a compound, the easier for it to donate an electron or capture a hole). However, in the presence of Pt nanoclusters nearby, methanol adsorption on TiO₂ ultimately leads to formation of H⁺ through photo-oxidation of methanol, and

Table 5. Solvent polarity of various alcohols tested.

Solvent	Polarity
Methanol	0.91
Ethanol	0.89
n-propanol	0.86
i-propanol	0.85
Butanol	0.84

eventually H₂, which is the key molecule for sensing of methanol by (TiO₂-Pt) NCs on GaN NW as explained in section 4.2. A similar argument holds for ethanol sensing by the GaN/(TiO₂-Pt) hybrids.

(3) Why is hydrogen detected only by GaN/(TiO₂-Pt) and GaN/Pt hybrids, and not by GaN/TiO₂ NWNC sensors, and why do GaN/(TiO₂-Pt) sensors have higher response to hydrogen than to alcohols?

From table 3, hydrogen has negligible heat of adsorption on TiO₂, thus GaN/TiO₂ devices are not sensitive to hydrogen. However, in the presence of Pt NCs on TiO₂, hydrogen can adsorb on the Pt NCs. Once adsorbed, hydrogen can modify the workfunction of Pt, resulting in a change in the photocurrent through the nanowire. However, this cannot be the only mechanism, as that would imply that GaN/Pt hybrids should be equally sensitive to H₂. It is likely that, when hydrogen is adsorbed on the TiO₂-Pt NC, it can also reduce the TiO₂ surface. Thus in the presence of only Pt on GaN, workfunction modification of Pt solely produces change in the photocurrent in the NW. However, in the presence of Pt and TiO₂ NCs, hydrogen adsorption leads to the modulation of the photocurrent in GaN NW, through modulation of Pt workfunction together with the change in the depletion layer of the TiO₂ NCs, resulting in a larger change of the photocurrent, and thus higher sensitivity.

The faster and larger response of GaN/(TiO₂-Pt) towards H₂ compared to the alcohols in figure 5 could be due to the fact that, in the case of alcohols, hydrogen is produced after photo-oxidation of the adsorbed alcohols, which is a two-step process with lower yield. In the case of H₂ in nitrogen, there is a direct availability of H₂ molecules.

(4) Why are GaN/(TiO₂-Pt) sensors not sensitive to high carbon-containing ($C > 2$) alcohols such as propanol and butanol?

It has been shown that the hydrogen production from the photocatalytic oxidation of alcohols on a TiO₂/Pt surface is related to the polarity of the alcohols, i.e. the higher the polarity of the alcohol the greater the yield of photocatalytic hydrogen production [25]. The polarity (Y) is defined as $Y = (\epsilon_s - 1)/(\epsilon_s + 2)$, where ϵ_s is the relative permittivity of the solvent. Table 5 lists the polarity of alcohols tested.

The relative difficulty of producing hydrogen from higher carbon-containing alcohols ($C > 2$) thus might be the cause of the GaN/(TiO₂-Pt) sensor's inability to detect alcohols with C greater than two. The sensor's greater response to methanol than ethanol (at least for concentrations above 500 $\mu\text{mol mol}^{-1}$) is also consistent with the polarities of the alcohols.

5. Conclusions

We have demonstrated that, by using metal and metal-oxide-based multicomponent NCs on GaN NWs, we can tailor the selectivity of GaN NW-based chemical sensors. We compared the behavior of three different kinds of NWNC hybrid sensor devices, i.e. GaN/(TiO₂-Pt), GaN/TiO₂ and GaN/Pt. It was shown earlier that GaN/TiO₂ sensors selectively detected aromatic compounds, such as benzene, toluene, chlorobenzene, ethylbenzene and xylene. In this study we found that, by adding Pt NCs to GaN/TiO₂ sensors, we can completely inhibit their sensitivity to the above-mentioned aromatic compounds. However, they start responding to hydrogen, methanol and ethanol. The GaN/Pt NWNCs on the other hand showed response only to hydrogen. The GaN/(TiO₂-Pt) hybrid sensors could be used for room-temperature hydrogen sensing, in various industrial production facilities, oil refineries and for hydrogen monitoring in hydrogen-powered vehicles. Also, these sensors could be used in alcohol monitoring systems for various industrial and law-enforcement purposes, such as in the production of alcohols-based bio-fuels and in breath analyzers.

This study indicates the potential of multicomponent NWNC-based sensors for developing the next generation of ultrasensitive and highly selective chemical sensors. Through combinations of metals and metal oxides available, we can produce a library of sensors, each with precisely tuned selectivity, on a single chip for detecting a wide variety of analytes in many different environments.

Acknowledgments

The George Mason University portion of this work was supported by the National Science Foundation under ECCS-0901712 grant. The University of Maryland portion of the work was partially supported by the Defense Threat Reduction Agency, Basic Research Award no. HDTRA1-10-1-0107, to the University of Maryland. VPO gratefully acknowledges the support from the NIST (contracts SB134110SE0579 and SB134111SE0814). We thank Dr Kurt Benkstein of NIST for sharing his design for the gas sensing set-up. We thank Dr Sergiy Krylyuk of NIST for his assistance in assembling the gas sensing setup. The nanowire devices were fabricated at the Nanofab clean room of the NIST Center for Nanoscale Science and Technology.

References

- [1] Wilson D M, Hoyt S, Janata J, Booksh K and Obando L 2001 *IEEE Sensors J.* **1** 256–74
- [2] Eranna G, Joshi B, Runthala D and Gupta R 2004 *Crit. Rev. Solid State Mater. Sci.* **29** 111–88
- [3] Cui Y, Wei Q, Park H and Lieber C M 2001 *Science* **293** 1289
- [4] Sberveglieri G, Baratto C, Comini E, Faglia G, Ferroni M, Ponzoni A and Vomiero A 2007 *Sensors Actuators B* **121** 208–13
- [5] Offermans P, Crego-Calama M and Brongersma S H 2010 *Nano Lett.* **10** 2412
- [6] Field C R, In H J, Begue N J and Pehrsson P E 2011 *Anal. Chem.* **83** 4724–8
- [7] Xue X (ed) 2008 *Nanowire Research Progress* 1st edn (New York: Nova Science Publisher)
- [8] Ramgir N S, Yang Y and Zacharias M 2010 *Small* **6** 1705–22
- [9] Joshi R K and Kruis F E 2006 *Appl. Phys. Lett.* **89** 153116
- [10] Mubeen S, Zhang T, Chartuprayoon N, Rheem Y, Mulchandani A, Myung N V and Deshusses M A 2010 *Anal. Chem.* **82** 250–7
- [11] Leghrib R, Pavelko R, Felten A, Vasiliev A, Cané C, Gràcia I, Pireaux J-J and Llobet E 2010 *Sensors Actuators B* **145** 411–6
- [12] Balázs C, Sedláčková K, Llobet E and Ionescu R 2008 *Sensors Actuators B* **133** 151–5
- [13] Kuang Q, Lao C-S, Li Z, Liu Y-Z, Xie Z-X, Zheng L-S and Wang Z L 2008 *J. Phys. Chem. C* **112** 11539–44
- [14] Zhang Y, Xu J, Xu P, Zhu Y, Chen X and Yu W 2010 *Nanotechnology* **21** 285501
- [15] Dobrokhotov V et al 2006 *J. Appl. Phys.* **99** 104302
- [16] Aluri G S, Motayed A, Davydov A V, Oleshko V P, Bertness K A, Sanford N A and Rao M V 2011 *Nanotechnology* **22** 295503
- [17] Calatayud M, Markovits A, Menetrey M, Mguig B and Minot C 2003 *Catal. Today* **85** 125–43
- [18] Royer S and Duprez D 2011 *ChemCatChem* **3** 24–65
- [19] Wang G C, Zhou Y H and Nakamura J 2005 *J. Chem. Phys.* **122** 044707
- [20] Somorjai G A 2010 *Introduction to Surface Chemistry and Catalysis* (New York: Wiley)
- [21] Conner W C, Pajonk G and Teichner S 1986 *Chem. Rev.* **95** 759
- [22] Hiehata K, Sasahara A and Onishi H 2007 *Nanotechnology* **18** 084007
- [23] Carp O, Huisman C and Reller A 2004 *Prog. Solid State Chem.* **32** 33–177
- [24] Morikawa T, Ohwaki T, Suzuki K, Moribe S and Tero-Kubota S 2008 *Appl. Catal. B* **83** 56–62
- [25] Yang Y Z, Chang C-H and Idriss H 2006 *Appl. Catal. B* **67** 217–22
- [26] Ruiz A M, Cornet A, Shimanoe K, Morante J R and Yamazoe N 2005 *Sensors Actuators B* **108** 34–40
- [27] Chen Y, Zhu C and Wang T 2006 *Nanotechnology* **17** 3012
- [28] Wu R-J, Huang Y-C, Yu M-R, Lin T H and Hung S-L 2008 *Sensors Actuators B* **134** 213–8
- [29] Brahim S, Colbern S, Gump R, Moser A and Grigorian L 2009 *Nanotechnology* **20** 235502
- [30] Liu J, Wang X, Peng Q and Li Y 2005 *Adv. Mater.* **17** 764–7
- [31] Ahn H, Park J-H, Kim S-B, Jee S H, Yoon Y S and Kim D-J 2010 *Electrochem. Solid-State Lett.* **13** J125–8
- [32] Wu W-Y, Ting J-M and Huang P-J 2009 *Nanoscale Res. Lett.* **4** 513
- [33] Xue X Y, Chen Y J, Liu Y G, Shi S L, Wang Y G and Wang T H 2006 *Appl. Phys. Lett.* **88** 201907
- [34] Chen Y J, Nie L, Xue X Y, Wang Y G and Wang T H 2006 *Appl. Phys. Lett.* **88** 083105
- [35] Sippel-Oakley J, Wang H-T, Kang B S, Wu Z, Ren F, Rinzler A G and Pearton S J 2005 *Nanotechnology* **16** 2218–21
- [36] Gong J, Sun J and Chen Q 2008 *Sensors Actuators B* **130** 829–35
- [37] Sun Y and Wang H H 2007 *Adv. Mater.* **19** 2818–23
- [38] Skucha K, Fan Z, Jeon K, Javey A and Boser B 2010 *Sensors Actuators B* **145** 232–8
- [39] Shen Y, Yamazaki T, Liu Z, Meng D and Kikuta T 2009 *J. Alloys Compounds* **488** L21–5

- [40] Bertness K A, Roshko A, Mansfield L M, Harvey T E and Sanford N A 2008 *J. Cryst. Growth* **310** 3154–8
- [41] Ioannides T and Verykios X E 1996 *J. Catal.* **161** 560–9
- [42] Zhdanov V P 2002 *Surf. Sci.* **512** L331–4
- [43] Heimer T A, Bignozzi C A and Meyer G J 1993 *J. Phys. Chem.* **97** 11987–94
- [44] Tang H, Prasad K, Sanjines R, Schmid P and Levy F 1994 *J. Appl. Phys.* **75** 2042–7
- [45] Garzella C, Comini E, Tempesti E, Frigeri C and Sberveglieri G 2000 *Sensors Actuators B* **68** 189–96
- [46] Wang H, Kang B, Ren F, Tien L, Sadik P, Norton D, Pearton S and Lin J 2005 *Appl. Phys. Lett.* **86** 243503
- [47] Lupan O, Ursaki V V, Chai G, Chow L, Emelchenko G A, Tiginyanu I M, Gruzintsev A N and Redkin A N 2010 *Sensors Actuators B* **144** 56–66
- [48] Yates J T Jr 2009 *Surf. Sci.* **603** 1605–12
- [49] Bikondoa O, Pang C L, Ithnin R, Muryu C A, Onishi H and Thornton G 2006 *Nature Mater.* **5** 189–92
- [50] Meyer G J, Lisensky G C and Ellis A B 1988 *J. Am. Chem. Soc.* **110** 4914–8
- [51] Anpo M, Tomonari M and Fox M A 1989 *J. Phys. Chem.* **93** 7300–2
- [52] Mansfield L M, Bertness K A, Blanchard P T, Harvey T E, Sanders A W and Sanford N A 2009 *J. Electron. Mater.* **38** 495–504
- [53] Kim K S and Barteau M A 1989 *Surf. Sci.* **223** 13–32
- [54] Fujishima A, Zhang X and Tryk D A 2008 *Surf. Sci. Rep.* **63** 515–82
- [55] Du X, Wang Y, Mu Y, Gui L, Wang P and Tang Y 2002 *Chem. Mater.* **14** 3953–7
- [56] Islam M M, Calatayud M and Pacchioni G 2011 *J. Phys. Chem. C* **115** 6809–14
- [57] Henderson M A, Otero-Tapia S and Castro M E 1999 *Faraday Discuss.* **114** 313
- [58] Zalkind S, Yakshinskiy B V and Madey T E 2008 *J. Vac. Sci. Technol. B* **26** 2241
- [59] Norton P R and Richards P J 1974 *Surf. Sci.* **44** 129
- [60] Sexton B A, Rendulic K D and Huges A E 1982 *Surf. Sci.* **121** 181
- [61] Saeys M, Reyniers M-F, Marin G B and Neurock M 2002 *J. Phys. Chem. B* **10** 7489–98
- [62] 2003 *CRC Handbook of Chemistry and Physics* 84th edn (Boca Raton, FL: CRC Press)